Hindawi
Mobile Information Systems
Volume 2022, Article ID 1203561, 12 pages
https://doi.org/10.1155/2022/1203561

Research Article

Quantitative of Atomic Spectra by Laser-Induced Teaching Integrating Multitarget Tracking Algorithm

Ying Zhang, Chunyu Liu, and Tingsong Zhang

Department of Physics, Changchun University of Science and Technology, Changchun, Jilin 130022, China

Correspondence should be addressed to Ying Zhang; zhangy@cust.edu.cn

Received 6 May 2022; Revised 21 June 2022; Accepted 17 August 2022; Published 14 September 2022

Academic Editor: Muhammad Muzammal

Laser-induced breakdown spectroscopy refers to the radiation spectrum formed by the vaporization and ionization of samples under high-temperature conditions. It is a new technology for detecting and analyzing the composition and content of materials. However, this technology is not yet very mature; in this regard, this paper proposes a quantitative study of atomic spectroscopy using laser-induced technology. On this basis, a method using laser-induced breakdown spectroscopy is proposed, and its quantitative analysis and application are carried out in detail. The laser-induced breakdown technology uses a high-power pulsed laser to form a plasma on the surface of the test piece and analyzes its radiation spectrum to obtain the composition and content of its elements. It also used the laser-induced breakdown technique to quantitatively analyze the Ti-doped Al_2O_3 ceramic system. Through the quantitative analysis of constant laser and constant plasma temperature, the linear correlation coefficient $R2$ of the calibration curve calculated with constant plasma temperature is obtained as 0.985, and the relative error is 5.3%. This paper uses a fixed laser pulse amplification voltage, the linear coefficient of the proportional relationship curve is only 0.92, and the error rate is 8.9%. By comparing the two curves, the Ti proportional curve obtained by a fixed plasma temperature is obtained in this paper. Its linearity is better than the Ti scaling curve obtained by constant laser voltage.

1. Introduction

Laser-induced breakdown spectroscopy (LIBS) is a component analysis and detection technology based on atomic absorption spectroscopy developed in the 1960s. This method uses high-power laser pulses to irradiate the material, so that the area irradiated by the laser vaporizes due to instantaneous absorption of a large amount of energy. It forms a large number of atoms and ions around the irradiated area, thereby forming a plasma. By analyzing the relationship between the intensity of the spectral lines and the wavelength (energy), it can determine the composition of the substance. Laser-induced breakdown spectroscopy has been widely used in various fields, such as environmental pollution detection, measurement of air pollution, and measurement of heavy metals in soil. LIBS has no requirements on the shape of the sample, and all solids, liquids, and gases can be tested by LIBS, so the application prospect is huge. At present, people have a certain understanding of the theory and application of laser-induced breakdown spectroscopy. However, problems such as the formation mechanism of laser-induced breakdown spectroscopy and the accuracy of quantitative analysis of measurement results have not been well resolved. In addition, the cost at that time was too high, and the performance of the detector was also restricted.

Due to the development of laser-induced fragmentation technology and LIBS technology, it has the characteristics of higher sensitivity, less sample pretreatment, and nondestructive testing. It has a wide range of applications in material analysis, industrial production control, archaeological and cultural relic identification, environmental monitoring, space exploration, biomedical assay analysis, etc. This paper explores the quantitative analysis of atomic spectroscopy based on laser-induced teaching integrating multitarget tracking algorithm, in order to make certain contributions to laser-induced breakdown spectroscopy technology.

In this paper, a quantitative analysis of atomic spectroscopy is carried out based on laser-induced teaching integrating multitarget tracking algorithm. The quantitative analysis of Al_2O_3-doped Ti ceramic system samples was carried out by laser-induced breakdown spectroscopy. By comparing the quantitative analysis of constant laser pulse voltage and constant plasma temperature, the linear correlation coefficient $R2$ of the calibration curve with constant plasma temperature is obtained as 0.985, and the relative error is 5.3%. Compared with the constant laser pulse increasing voltage, the correction curves obtained in this paper have only 0.92 and 8.9% errors. By comparison, it is found that the Ti calibration curve obtained by keeping the plasma temperature constant is more linear than the curve obtained by keeping the laser voltage constant.

The innovations of this paper are as follows: (1) this paper introduces the laser-induced breakdown spectroscopy technique. (2) This paper analyzes and discusses the multiobjective algorithm based on multifeature fusion. (3) In this paper, the precise quantitative analysis and application of laser-induced breakdown spectroscopy are carried out. The quantitative analysis and research of Al_2O_3-doped Ti ceramic system samples are carried out by laser-induced breakdown spectroscopy.

2. Related Work

According to the research progress in foreign countries, different researchers have conducted corresponding cooperative research on laser-induced breakdown spectroscopy. Liu et al. [1] presented digital imaging results of urea crystal growth after laser-induced nucleation. The results overturn the results of theoretical and experimental studies that have long influenced NPLIN [1]. Khan et al. [2] results obtained using laser-invited breakdown spectrum (LIBS) were shown in comparison with those obtained using induced currents by inductively coupled plasma transmission spectrum (ICP). He found that the concentration of certain elements (Ba and Cr) was higher than the allowable safety limit. He also discussed the health risks associated with exposure to such toxic elements [2]. Lepeshov et al. [3] proposed and demonstrated a novel hybrid oligomer. The oligomer consists of unsymmetrical metal-dielectric (Au/Si) nm, and this hybrid nanoparticle oligomer can be fine-tuned by fs laser-induced fusion of nanoscale gold nm to achieve Fano resistance [3]. Yan et al. [4] research was designed to examine the impact of hematoporphyrin dimethyl ether (HDME)-mediated photodynamic treatment on laser-induced plexiform choroidal neovascularization (CNV) in mature Brown Norway mice [4]. Laser-induced fluorescence spectroscopy has the characteristics of high sensitivity, and fast and accurate monitoring. In order to identify water inrush, Wang et al. [5] introduced laser-induced fluorescence spectroscopy technology to obtain water inrush fluorescence spectral data [5]. However, these scholars still lack a certain technical demonstration on the research of laser-induced breakdown spectroscopy. After research, it is found that the quantitative analysis of laser-induced breakdown spectroscopy based on the fusion multitarget tracking algorithm has certain reliability.

At present, scholars have conducted in-depth research on multitarget tracking algorithms. Zhang et al. [6] proposed a new adaptive image tracking method based on multiple features. He designed a robust appearance model to overcome distractions in videos by fusing powerful features such as gradient histograms, local binary patterns, and color naming at the response map level [6]. In order to make full use of the diversity of samples during tracking and enhance the universality of tracking, Zhang et al. [7] combined the prediction results of the target model with the Staple method. And he used the weight bands to simplify the linearity to get different predicted responses. Li et al. [8] used object detection technology and deep residual network (ResNet) to extract comprehensive features of clothing. Its purpose is to focus on the clothing itself during the feature extraction process. Based on this, he introduced a multi-level feature information fusion method based on multi-level features [7, 8]. He et al. [9] proposed a multi-object tracking method using a distributed camera network [9]. Based on machine learning algorithms, Max [10] studied a fixed-point tracking model for English reading texts based on mean shift and multifeature fusion. Through repeated iterations of the vector, he obtained the offset vector and finally made it converge to the actual position to achieve the tracking of the target [10]. However, these scholars have not explored the quantitative analysis of atomic spectra based on laser-induced teaching integrating multitarget tracking algorithms. It is only a one-sided discussion of its meaning.

3. Quantitative Method of Atomic Spectrum

In this paper, the quantitative analysis of metal oxides is carried out. The intensity of the atomic emission spectrum of the element is closely related to the plasma temperature and the concentration of the element in the sample. Under the condition that the plasma temperature remains unchanged, the calibration curve can be obtained according to the relationship between the element breakdown line intensity and the element concentration in the sample, so as to measure the element concentration. However, in the actual laser-induced breakdown spectroscopy test, it is difficult to keep the plasma temperature fixed for the following reasons: first, the internal parameters of the laser vary. Since the energy of each laser pulse cannot be exactly the same, the resulting plasma temperature is also different. Again, as the laser burns the sample, grooves are created on the surface of the sample. The plasma energy generated by the excited atoms and ions inside the groove will be absorbed by the sample, resulting in different plasma temperatures. Finally, the components in the samples are different. The plasma temperature is also different due to the different ionization rates excited by the laser. In this paper, the quantitative analysis of Al_2O_3-doped Ti ceramic system samples was carried out by laser-induced breakdown spectroscopy. In the experiment, in order to obtain the temperature of the plasma generated by the laser breakdown, the ratio of the characteristic peaks of two Al atoms was selected for real-time monitoring, and

the plasma temperature could be maintained by continuously adjusting the pulse amplification voltage of the laser. This method overcomes the inherent drawbacks of laser-induced breakdown spectroscopy, which is more accurate than the scaling curves obtained by traditional methods using constant laser pulse amplification voltage. In this paper, the quantitative analysis of atomic spectra is explored based on laser-induced teaching integrating multitarget tracking algorithm.

3.1. Laser-Induced Breakdown Spectroscopy. The laser-induced breakdown technology uses a high-power pulsed laser to form a plasma on the surface of the specimen and analyzes its radiation spectrum to obtain the composition and content of its elements [11]. The simplest and most typical measurement system is shown in Figure 1, where a high-energy-density laser pulse is focused on the surface of the specimen. When the power density reaches or exceeds 1 kW/cm^2, the material in the laser focus area on the surface of the material sample will be heated to 10,000 degrees Celsius in an instant. It produces evaporation and expansion, which produces a small fraction (micrograms) of the substance, which is called laser ablation. Due to the absorption of a large amount of laser energy, the temperature of the material in the laser ablation area rises rapidly, and a gas composed of electrons, ions, atoms, molecules, and other particles is formed within the laser irradiation range. Under the impact of free electrons and subsequent laser pulses, this mass of gaseous matter finally produces a high-temperature, high-voltage plasma composed of electrons, ions, and atoms. The spectrum of these plasmas is focused and attached to the fiber and sent to a detector, which displays the collected spectral lines on a display.

During the laser pulse, the laser heats up the plasma rapidly, locally up to 100,000 K. The duration of the laser pulse is usually several to 10 nanoseconds, so the reaction time of the laser pulse and the material is very short. When the pulsed laser reacts with the matter, the particles in the plasma collide with each other, thus reaching a local thermal equilibrium, whose equilibrium temperature drops to about 10,000 K. After reaching the equilibrium state, the ions get sufficient energy and expand around in the form of a hemisphere. During this period, the temperature of the plasma gradually decreases. Plasma radiation during this period is dominated by blackbody light, visible light, near-infrared light, and shifts in red over time. This connection spectrum decays rapidly with time, and its decay time is between 1 and 2 μs [12]. After 10 microseconds, the temperature of the plasma begins to drop, and at this time, the radiation is mainly a mixed radiation of ions and electrons, showing a spectrum from ultraviolet to visible.

3.2. Multiobjective Algorithm Based on Multi-Feature Fusion. Multitarget tracking is an important research object in the field of computer vision. Based on the detected target, it is matched with the existing trajectory data [13]. It records the moving track of the target in real time. It records the disappearing target trajectory in time and destroys the corresponding trajectory. It judges new targets in time and establishes new track objects.

In recent years, with the introduction of deep convolutional neural networks, people have increasingly realized its powerful feature expression capabilities. At present, it has been used in almost all fields of computer vision, including target detection, target tracking, and target segmentation.

Through massive data learning, the convolutional features of deep neural networks can be compared with traditional manual features, and a series of features such as position features, scale features, and rotation features can be learned. It has a better comprehensive representation of the same target, and it provides better support for data matching for multitarget tracking [14]. Figure 2 shows the multifeature fusion algorithm.

3.2.1. State Characteristics. Here, we use the extended Kalman filter to estimate the motion state of the target, such as position, velocity, and acceleration [15]. The Kalman filter is mainly used to estimate the system state in an uncertain dynamic system including interference and other factors. It has the advantages of fast operation speed and low operation cost.

For time s, the system state $A(s)$ satisfies the formula

$$A(s) = G(s) * A(s-1) + R(s). \tag{1}$$

$A(s)$ is the system state at time s, $R(s)$ is the system noise at time s, and $G(s)$ is the system parameter. And for the system state $A(s)$, the measurement formula needs to be satisfied

$$C(s) = K * A(s) + W(s). \tag{2}$$

Among them, $C(s)$ is the measurement value at time s, K is the measurement function of the corresponding state of the system, and $W(s)$ represents the measurement noise.

In the above formula, the uncertainty of the system at time s is given and transmitted by the covariance matrix $\varepsilon(s)$,where the uncertain transfer satisfies the state transition matrix:

$$\varepsilon(\overline{s}) = G(s) * \varepsilon(s-1) * G(s)^S + U(s). \tag{3}$$

Here, $U(s)$ is the process noise of the system. Due to the uncertainty in the formula of state, according to the Kalman filter, a relatively correct system satisfies

$$\widehat{A}(s) = \widehat{A}(\overline{s}) + L_s * (C(s) - K * A(\overline{s})). \tag{4}$$

Here, $\widehat{A}(s)$ represents the estimated value of the system state at time s, L_s is the Kalman gain coefficient in the Kalman filter, and $C(s) - K * A(\overline{s})$ represents the residual between the actual observed value and the estimated value. Finally, the error of the system mean square error is zero. Kalman gain derivation can be obtained

$$L_s = \varepsilon(s)K^S\left(K\varepsilon(s)K^S + E\right)^{-1}. \tag{5}$$

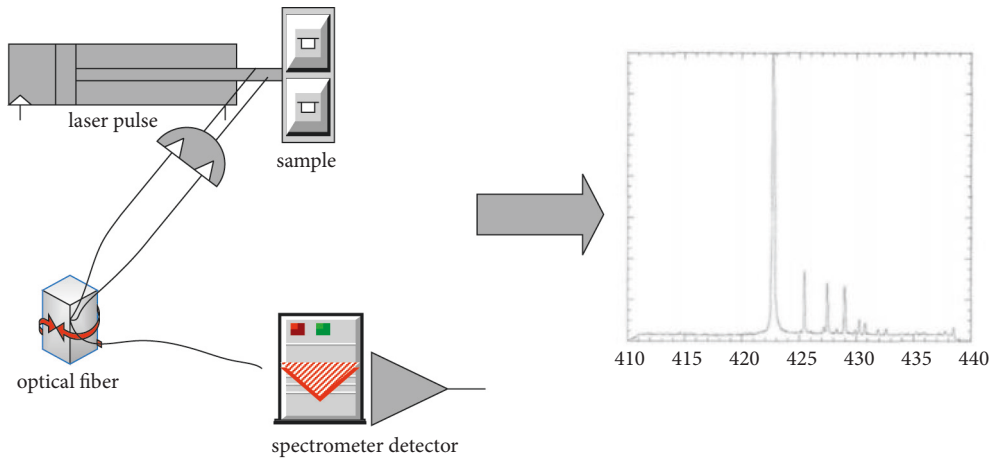

Figure 1: Schematic diagram of the LIBS system.

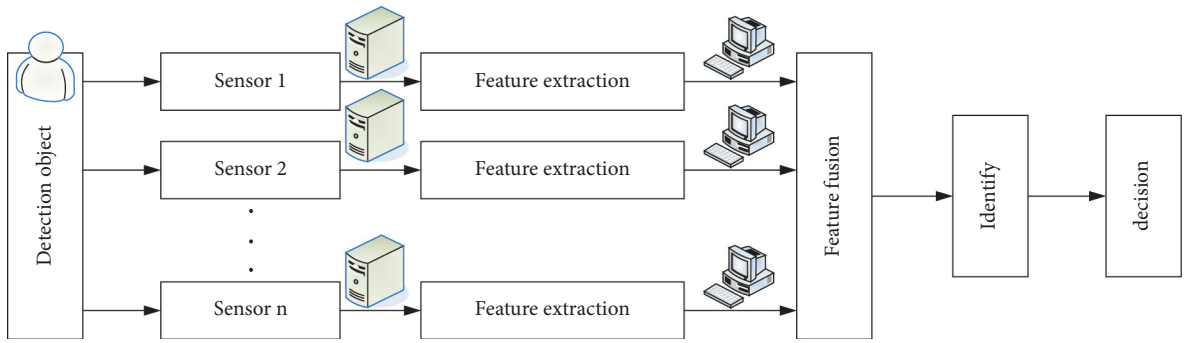

Figure 2: Multifeature fusion algorithm.

E represents the instrument noise error during the measurement process, and $\varepsilon(s)$ can be obtained correspondingly to satisfy the formula

$$\varepsilon(s) = (N - L_s K)\varepsilon(\bar{s}). \tag{6}$$

The target motion between two adjacent frames in the video can be approximately regarded as uniform motion, and its kinematics formula is as follows. Δs is the time interval between adjacent frames:

$$\begin{aligned} I_s &= I_{s-1} + \Delta s J_{s-1}, \\ J_s &= J_{s-1}. \end{aligned} \tag{7}$$

In summary, using the Kalman filter, according to the position and scale set of the detection candidates of the previous frame, the state vector of the Kalman filter is set as follows:

$$A_{v_n} = \{v_n\}_n^P. \tag{8}$$

Among them

$$v_n = \left(a_{v_i}, b_{v_i}, u_{v_i}, k_{v_i}, j_{av_i}, j_{bv_i}\right), \tag{9}$$

a_{vn} and b_{vn} represent the coordinates of the upper left corner of the target, u_{v_i} and k_{v_i} represent the width and height of the target rectangle, respectively, and j_{v_i} represents the scalar velocity of the center point of the target, which is derived from the formula $j = \sqrt{\Delta a^2 + \Delta b^2}$. Thus, its state transition matrix is as follows:

$$G(s) = \begin{bmatrix} 1 & 0 & 0 & 0 & \Delta s \\ 0 & 1 & 0 & 0 & 0 \\ 0 & 0 & 1 & 0 & 0 \\ 0 & 0 & 0 & 1 & 0 \\ 0 & 0 & 0 & 0 & 1 \end{bmatrix}. \tag{10}$$

According to the rectangular frame information of the target, the observation vector and observation matrix can be obtained as follows. $a_c(s)$, $b_c(s)$, $u_c(s)$, and $k_c(s)$ represent the upper left corner coordinates and width and height of the target rectangular frame, respectively,

$$\begin{aligned} C(s) &= \begin{bmatrix} a_c(s) \\ b_c(s) \\ u_c(s) \\ k_c(s) \end{bmatrix}, \\ K &= \begin{bmatrix} 1 & 0 & 0 & 0 & 0 \\ 0 & 1 & 0 & 0 & 0 \\ 0 & 0 & 1 & 0 & 0 \\ 0 & 0 & 0 & 1 & 0 \end{bmatrix}. \end{aligned} \tag{11}$$

After the above formulas are sorted, the state and observation formulas can be re-described. On this basis, $R(s)$ and $J(s)$ are $5 * 1$ and $4 * 1$ system noises, respectively, which are both Gaussian noises with an average value of 0. The covariance matrices W and E of system noise and observation noise are, respectively, set as follows:

$$W = \begin{bmatrix} 1 & 0 & 0 & 0 & 0 \\ 0 & 1 & 0 & 0 & 0 \\ 0 & 0 & 1 & 0 & 0 \\ 0 & 0 & 0 & 1 & 0 \\ 0 & 0 & 0 & 0 & 1 \end{bmatrix}, \quad E = \begin{bmatrix} \varphi_a^2 & 0 & 0 & 0 \\ 0 & \varphi_b^2 & 0 & 0 \\ 0 & 0 & \varphi_u^2 & 0 \\ 0 & 0 & 0 & \varphi_k^2 \end{bmatrix}. \tag{12}$$

Setting the variance $\varphi_a^2 = \varphi_{\mathrm{b}}^2 = \varphi_{\mathrm{u}}^2 = \varphi_{\mathrm{k}}^2 = 1$ of the four components of the observation noise in the above formula, then the observation noise covariance matrix E is the identity matrix. In addition, the initial value of the error covariance matrix can be set as follows:

$$\varepsilon(\overline{s}) = \begin{bmatrix} 0.0004 & 0 & 0 & 0 & 0 \\ 0 & 0.0004 & 0 & 0 & 0 \\ 0 & 0 & 0.0004 & 0 & 0 \\ 0 & 0 & 0 & 0.0004 & 0 \\ 0 & 0 & 0 & 0 & 0.0004 \end{bmatrix}. \tag{13}$$

Because the motion of the target in adjacent frames is approximate to a uniform motion, for the convenience of calculation and after testing, let the frame interval $\Delta s = 0.04$.

Finally, according to the position and scale set $A_{v_n} = \{v_n\}_n^P$ of the detection candidate frame of the previous frame, the position and scale set $T = \{t_m\}_m^Q$ of the prediction candidate frame of the next frame are estimated, among them

$$t_m = \left(a_{t_m}, b_{t_m}, u_{t_m}, k_{t_m}, j_{t_m}\right). \tag{14}$$

Then, the calculation method of the state feature similarity between targets is as follows:

$$O_{status}\left(v_n, t_m\right) = e^{-\left\|\left(v_n - t_m\right)\right\|^2}. \tag{15}$$

3.2.2. Location Scale Features. $d_m = (a_{t_m}, b_{t_m}, u_{t_m}, k_{t_m})$ in the position and scale set of the prediction candidate frame of the next frame predicted according to the Kalman filter, and $d_n = (a_{v_n}, b_{v_n}, u_{v_n}, k_{v_n})$ in the position and scale set of the detection candidate frame of the previous frame. We calculate the IOU of the two candidate boxes as their location scale features. The specific calculation method is as follows:

$$O_{location}\left(d_n, d_m\right) = \frac{area\left(d_n \cap d_m\right)}{area\left(d_n \cup d_m\right)}. \tag{16}$$

Among them, $area(\bullet)$ represents the area.

3.2.3. Multifeature Fusion Algorithm. It can be seen from the above analysis that the appearance feature focuses on the similarity of the appearance of the target, and the state feature focuses on the similarity of the information such as the motion state and the position state between the targets. The position scale state focuses on the overlap of candidate regions between objects. Accordingly, the linear fusion features of these three features are used at the same time, and comparative experiments are carried out with different linear ratios. The specific formula is as follows:

$$O(n, m) = \gamma * O_{appearance}(n, m) + \sigma * O_{status}\left(v_n, t_m\right) + \tau * O_{location}\left(d_n, d_m\right). \tag{17}$$

Different from single-target tracking, it narrows the search area of the next frame according to the response results of the previous frame. The main difficulty of detection-based multitarget tracking is how to perform data matching, which may occur in the following situations: (1) false matching due to the similarity of faces in the video. (2) The false detection and missed detection of faces due to the error of the detector lead to the target tracking error in the data matching process. (3) The target occludes during the video process or leaves the video area for a short time. Its reset matches after the target reappears. (4) Record new detection targets and disappeared detection targets in time, and establish or destroy corresponding tracking records. On the other hand, due to the large amount of computation of the convolutional neural network, in the online multitarget tracking process, we hope to obtain the corresponding apparent features in a short time.

Accordingly, this paper proposes a multitarget tracking algorithm based on multifeature fusion. Through the multifeature fusion of apparent features, state features, and location scale features, combined with a data matching method based on redefinition, multitarget tracking is performed. We also discuss the quantitative analysis of atomic spectra based on the fusion of multitarget tracking algorithm laser-induced teaching. In the following, further experimental studies are carried out on the laser-induced and quantitative analysis of atomic spectroscopy.

4. Experimental Results

4.1. Elemental Detection of Al_2O_3-TiO_2 Samples. The sample to be tested in the test is a compound in which Al_2O_3 powder is mixed with TiO_2 powder in different proportions. The

preparation process of the sample is as follows: first, it weighs 8 g of Al_2O_3 powder mixed with an appropriate amount of TiO_2 nanoparticles (20–40 nm in diameter). According to the atomic percentages of TiO_2 and Al_2O_3 of 0.5 : 100, 1 : 100, 2 : 100, 3 : 100, and 4 : 100, the weights of the TiO_2 particles were weighed to be 0.0778 g, 0.1553 g, 0.3128 g, 0.4676 g, and 0.6257 g, respectively. It mixes Al_2O_3 powder and TiO_2 powder uniformly and labels AT05, AT10, AT20, AT30, and AT40 accordingly. In this paper, the obtained five groups of powders were added with an appropriate amount of deionized water, and then ball milled in a ball mill for 20 hours to mix TiO_2 and Al_2O_3 evenly. Finally, it grinds the dry powder, presses it into disks with a diameter of 12 mm and a thickness of 5 mm, and then sinters it at a temperature of 600°C to form a hard sample. It prepared samples with 0.2, 0.4, 0.6, and 0.8 atomic percent Ti and Al, respectively (labeled AT02, AT04, AT06, and AT08, respectively) using the same method. The results are shown in Tables 1 and 2.

In this paper, the sample is subjected to laser breakdown, the ambient gas is air, and the amplification voltage of the laser pulse is adjusted from 200 V to 700 V. Adjusting every 50 V, set the laser frequency to 10 Hz, and set the laser wavelength to 1064 nm. It sets the integration time and scan times of the spectrometer to 200 ms and 50 times, respectively. In this paper, the spectrogram shown in Figure 3 is obtained. Due to the laser breakdown experiments performed in the air environment, the emission spectra of nitrogen and oxygen elements in the air are inevitably excited. Therefore, the detection of nitrogen and oxygen in the sample will be affected (this sample does not contain nitrogen, so it is not affected by nitrogen in the air).

From the figure, many characteristic peaks can be found, among which the emission peaks of nitrogen, oxygen, aluminum, and titanium are the main ones. Since the ambient gas of the laser-induced breakdown spectroscopy is air, it has a strong background radiation, which interferes with the accurate detection of the elements in the compound. However, ASD can still be consulted to obtain several strong characteristic spectra of Al and Ti elements in the Al_2O_3-TiO_2 sample. Since the characteristic spectrum of oxygen in the compound overlaps with the emission spectrum of oxygen in air, it is difficult for us to identify oxygen in the compound.

4.2. Quantitative of Al_2O_3-TiO_2 Samples

4.2.1. Influence of Burning Conditions on Plasma Temperature and Calibration Curve. It mainly studies the effect of burning conditions on the plasma temperature by two methods: fixing the laser pulse amplification voltage and changing the laser burning point in real time. The experimental sample is AT05 (the atomic percentage of Ti and Al is 0.5 : 100), the laser pulse amplification voltage is set to 300 V, the integration time of the spectrometer is 200 ms, and the average scan is 50 times. In the experiment, the laser cauterized AT05 for 1000 times and collected every 50 times of cauterization. In the case of a fixed laser pulse amplification voltage, it is obtained that the effects of cautery and plasma temperature and scaling curves are shown in Figure 4.

Table 1: Sample contents of different Ti/Al in Al_2O_3-TiO_2 system 1.

Numbering	Al_2O_3 content (g)	TiO_2 content (g)	Ti/Al (%)
AT02	8	0.0308	0.2
AT04	8	0.0617	0.4
AT05	8	0.0778	0.5
AT06	8	0.0936	0.6

Table 2: Sample contents of different Ti/Al in Al_2O_3-TiO_2 system 2.

Numbering	Al_2O_3 content (g)	TiO_2 content (g)	Ti/Al (%)
AT08	8	0.1218	0.8
AT010	8	0.1553	1
AT020	8	0.3128	2
AT030	8	0.4676	3
AT040	8	0.6257	4

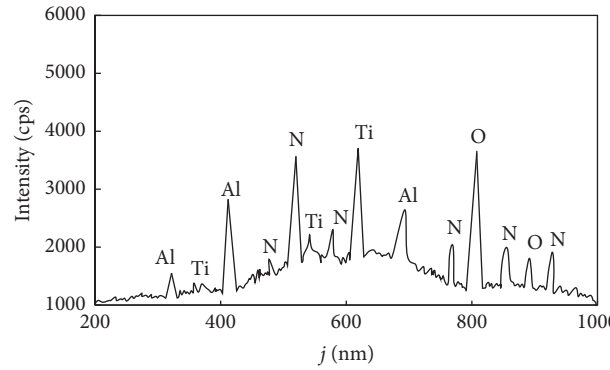

Figure 3: Laser-induced breakdown spectra of Al_2O_3-TiO_2 samples in air.

It shows that the laser burning position has a great influence on the plasma temperature; that is, the burning depth of the sample has a great influence on the plasma temperature. The plasma temperature varies greatly in the initial stage. This is because in the initial stage of plasma formation, the plasma has not yet reached a local thermal equilibrium state. It is just a thermodynamic energy exchange process in which ion atoms collide with each other in the plasma, and the plasma pressure in the groove changes rapidly at this time. Internal plasma pressure changes cause changes in the electron density of the plasma, thereby affecting the state of the plasma. It can be found that different cauterization depths have a great influence on the calibration curve, which is mainly because the plasma temperature fluctuates within a certain range due to different cauterization depths. Moreover, different elements have different ionization rates under the excitation of the same laser energy, so the ratio of the spectral line intensity of Ti atoms to that of Al atoms varies with the plasma temperature.

In order to reduce the effect of the burning point on the plasma temperature, it is necessary to ensure that the laser pulses burn the sample surface uniformly, which can be achieved by rotating the sample through a stepper motor. In

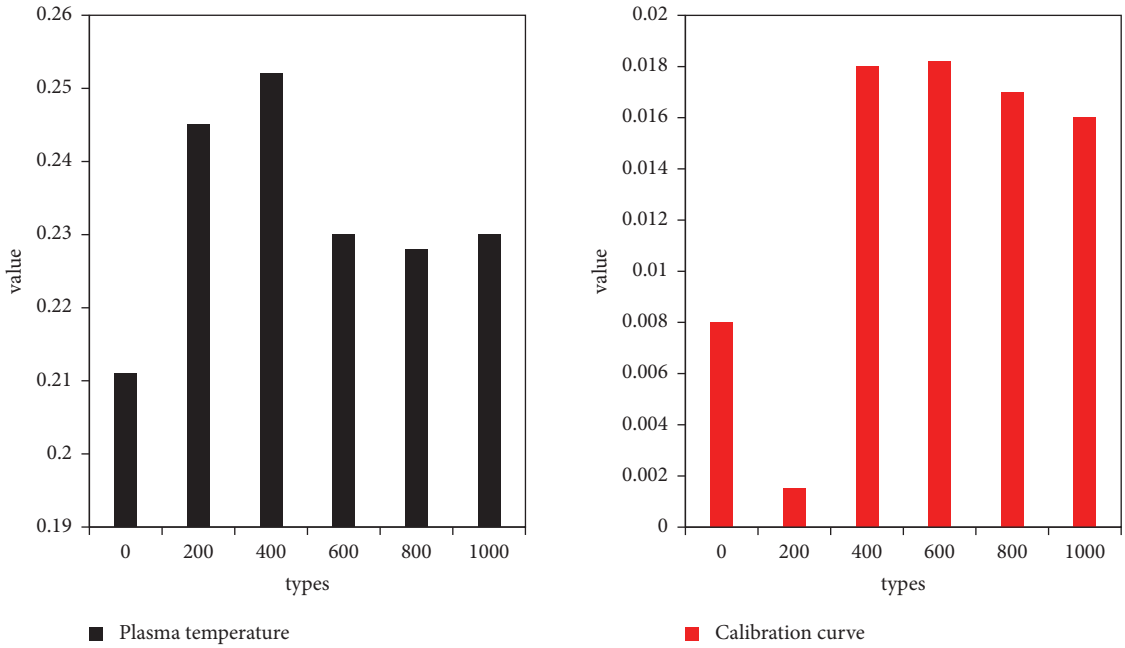

Figure 4: Effect of laser burning on plasma and calibration curve when laser amplification voltage is fixed.

the experiment, AT05 was used as the sample, and other experimental parameters remained unchanged except that the number of laser cauterization was changed to 550 times. When the laser burning point is changed in real time, the obtained results of laser burning and plasma temperature and calibration curve are shown in Figure 5, respectively.

The figure illustrates that the plasma temperature fluctuates in a small range while changing the laser ablation position in real time. At the same time, it was confirmed that by moving the sample surface in real time when laser cauterization occurred on the sample surface, the influence of cauterization conditions on the plasma temperature and the calibration curve could be reduced. This also provides a feasible method for the constant plasma temperature method, which provides a basis for obtaining high-precision calibration curves subsequently.

4.2.2. Influence of Laser Pulse Energy on Plasma Temperature and Calibration Curve. The experimental samples are samples AT05-AT40, the laser pulse frequency is set to 10 Hz, and the integration time of the spectrometer is 200 ms. The number of scans was set to 50, and the amplification voltage of the laser pulse was adjusted between 200 V (laser energy of 400 mJ) to 700 V (laser energy of 1400 mJ). It collects the ratio of the Al I peak intensity corresponding to 308.2 nm and the Al I characteristic spectrum intensity of 396.2 nm every 50 volts, and the obtained relationship between the plasma temperature and the laser pulse energy is shown in Figure 6.

It can be seen from the figure that AT05-AT40 five groups of samples are doped with different contents of Ti under the action of the same laser pulse energy, and the plasma temperature generated on the surface of the samples is different. This is mainly due to the influence of matrix effects. The absorption efficiency and scattering efficiency of the trace element Ti in the samples are different for laser rays, resulting in different plasma temperatures. It can also be found that under a certain laser amplification voltage, the plasma temperature will increase with the increase of the laser pulse amplification voltage, and the plasma temperature will decrease as the laser pulse voltage continues to increase. This is mainly because as the laser pulses continue to burn the same point on the sample surface, the surface atoms or molecules of the sample evaporate to produce grooves of different depths. In the initial stage, the laser-amplified voltage plays a major role in increasing the plasma temperature. When the voltage is greater than 600 volts, the laser pulse is focused on the sample surface in the groove so that the plasma temperature generated on the surface will transfer heat to the surrounding gas and the atoms in the groove. And the focal point of the high-energy laser pulse is deviated from the surface of the sample. The quantitative analysis of laser-induced breakdown spectroscopy is the analysis of plasma ions or atoms, so the calibration curves obtained under different plasma states are also different. The effects of different laser amplification voltages on the calibration curves of five groups of samples, AT05, AT10, AT20, AT30, and AT40, were experimentally studied, and the results are shown in Figure 7.

It can be seen from the figure that the ratio of the Ti I peak intensity corresponding to 453.3 nm and the Al I peak intensity corresponding to 396.2 nm increases with the increase of laser energy. The ITi I/IAl I I increases with increasing Ti and Al atomic percentages. This is mainly because the different atomic structures of Ti and Al make their ionization rates different, and the absorption rates of laser energy are different for samples doped with different Ti

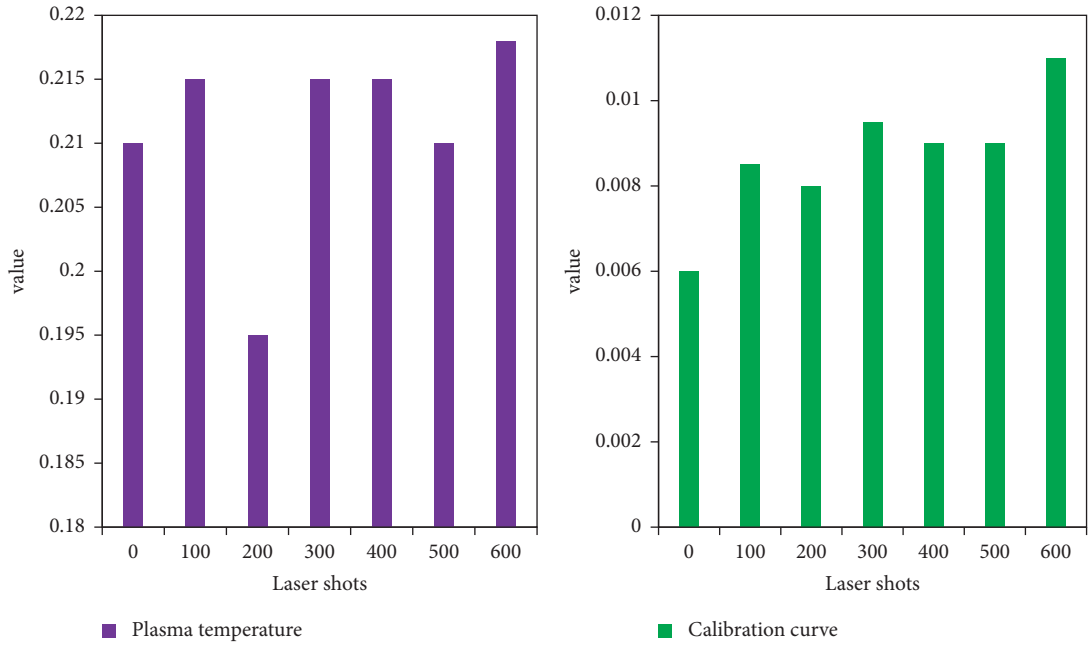

Figure 5: Effect of laser cautery on plasma temperature and calibration curve when the laser cautery point is changed in real time.

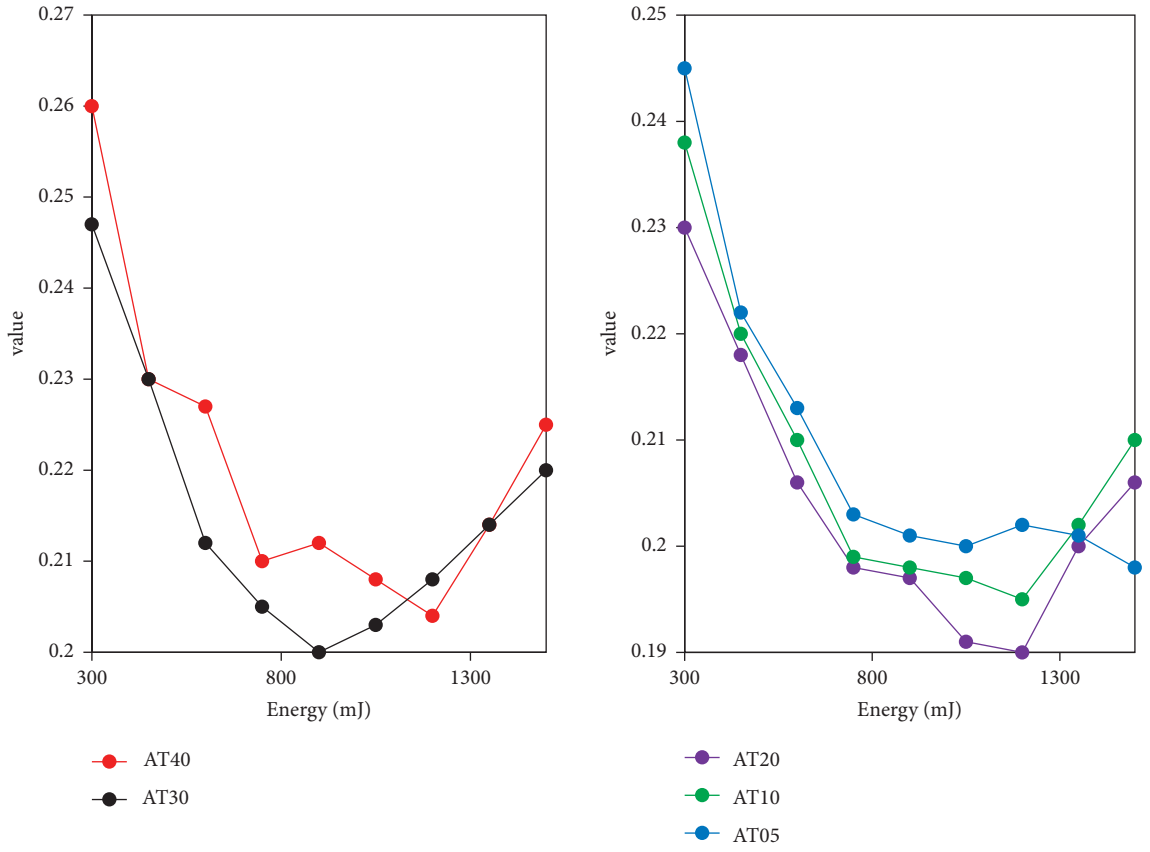

Figure 6: Effect of laser pulse energy on plasma temperature.

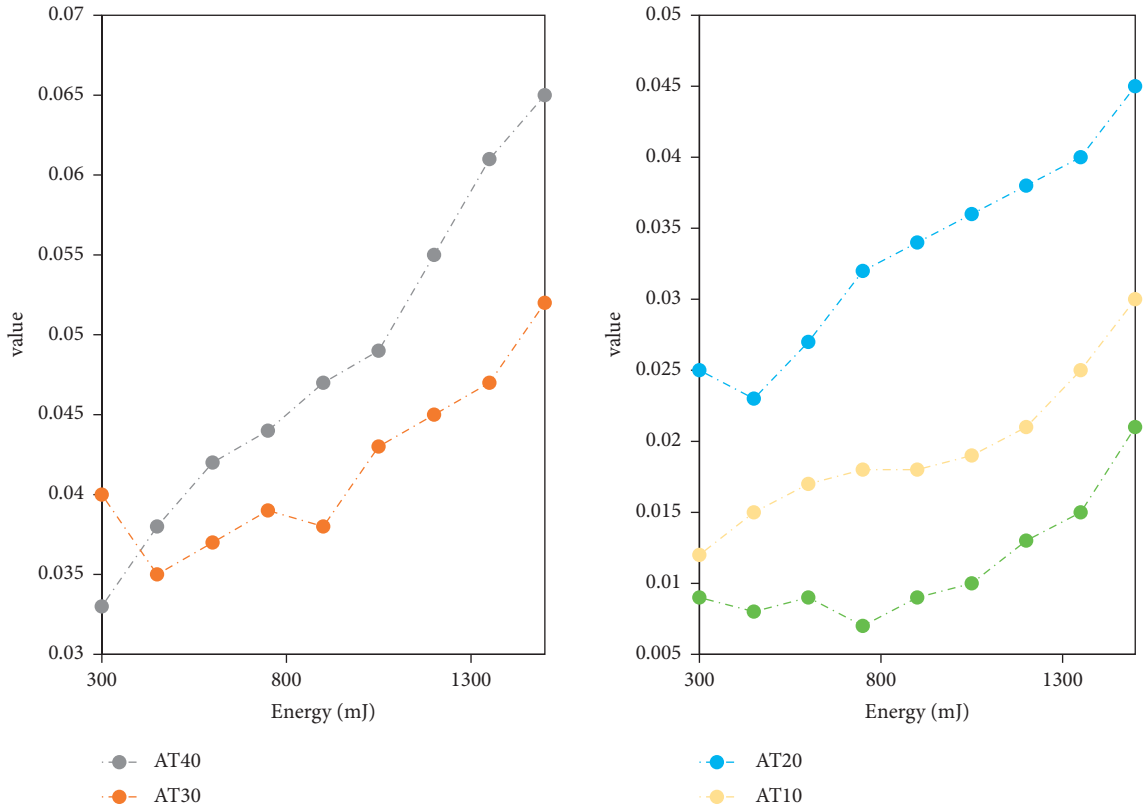

Figure 7: Effect of laser pulse energy on calibration curve.

contents. With the increase of laser pulse energy, the absorption rate of Ti atoms to laser energy increases faster than that of Al atoms, so that ITi I/IAl I increases with the increase of laser amplification voltage.

4.3. Quantitative of TiO_2-SiO_2 Ceramic Samples by Laser-Induced Breakdown Spectroscopy

4.3.1. Qualitative Analysis of Ceramic Samples of TiO_2-SiO_2 System. The experimental samples are six groups of ceramic samples with different Ti/Si ratios. The preparation process is as follows: first, it weighs 10 g SiO_2 powder, respectively. It weighs an appropriate amount of TiO_2 particles according to the atomic percentages of TiO_2 and SiO_2 at 0.5 : 100, 1 : 100, 2 : 100, 3 : 100, 4 : 100, and 5 : 100, and mixes SiO_2 powder and TiO_2 powder evenly. The six groups of powders obtained were added with an appropriate amount of deionized water, respectively, and put into a ball mill for ball milling for 20 hours, and the obtained solution was placed in a drying oven at 80°C for 20 hours. Finally, it grinds the dried powder, presses it into disks with a diameter of 12 mm and a thickness of 5 mm, and then sinters it into a hard ceramic sample in a single-crystal furnace at 1100°C. The element contents in each group of samples in the experiment are shown in Tables 3 and 4.

The S1-type sample was used for the test, and the breakdown was performed in the atmosphere, with a laser pulse of 200 volts, an operating frequency of 10 Hz, a laser wavelength of 1064 nm, a spectrometer of 100 milliseconds, and 25 scans. During the test, in order to prevent the ablation of the surface of the sample by the laser beam, it must move the sample to different positions in real time. It thus causes the components and contents in the sample to have an uneven distribution on the surface of the sample. By averaging the radiation spectra of different regions of the sample surface, it can reduce the measurement error of the sample to a certain extent. The resulting emission spectrum is shown in Figure 8.

It can be seen from the figure that the emission spectrum of TiO_2-SiO_2 ceramics in air is more, the characteristic peaks of Ti are obviously more than those of Si, and the spectral line intensity of Ti is obviously higher than that of Si. This is because the emission sensitivity coefficient of metal Ti atoms excited by laser is greater than that of silicon. Due to the laser breakdown experiment in air, there are inevitably some interference peaks of nitrogen and oxygen, but it is still possible to query the atomic spectrum database to obtain several obvious characteristic peaks of Ti and Si. There are mainly Si I peak near 251 nm, 288.16 nm corresponding to Si I peak, 323 nm and 334 nm combined Ti characteristic peak, 412.8 nm Si II ion peak, and 634.7 nm and 637.13 nm both correspond to Si II. In addition, those characteristic peaks before 500 nm are mainly characteristic peaks of Ti element.

4.3.2. Quantitative Analysis of Ceramic Samples of TiO_2-SiO_2 System. This paper mainly analyzes the Ti content in TiO_2-SiO_2 system ceramics. Due to the high hardness of the TiO_2-SiO_2 system ceramics, it is generally not conductive, and it is

Table 3: Contents of TiO_2-SiO_2 ceramic samples with different ratios 1.

Numbering	TiO_2 powder content (g)	SiO_2 powder content (g)	Ti/Si atomic ratio
*S*1	0.0556	8	0.5/100
*S*2	0.0872	8	1/100
*S*3	0.1673	8	2/100

Table 4: Contents of TiO_2-SiO_2 ceramic samples with different ratios 2.

Numbering	TiO_2 powder content (g)	SiO_2 powder content (g)	Ti/Si atomic ratio
*S*4	0.2462	8	3/100
*S*5	0.3212	8	4/100
*S*6	0.4213	8	5/100

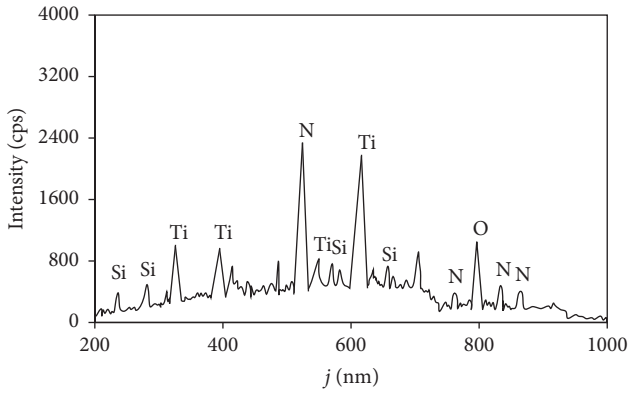

Figure 8: LIBS emission spectrum of TiO_2-SiO_2 ceramics in air.

difficult to test the composition and content by the commonly used composition analysis methods. In the quantitative analysis of LIBS, the plasma temperature is a key factor affecting the accuracy of quantitative analysis, and the plasma temperature is generally characterized by the ratio of the intensities of the two spectral lines of the same element in the same ionization state. The experiment moves the sample in real time, which makes the laser beam burn at different points on the sample surface to reduce the influence of matrix effects and burning conditions on the calibration curve.

In the experiment, the calibration curve of Ti in SiO_2-TiO_2 system ceramics was obtained by comparing the two methods of constant laser pulse amplification voltage and constant plasma temperature. Since the plasma temperature cannot be directly read by observing the laser-induced emission spectrum during the experiment, the change in plasma temperature was indirectly observed by observing the intensity ratio of the Si I288.7 nm and Si I251.4 nm lines in the experiment. The plasma temperature changes of the S3 sample observed under the laser pulse voltage of 300 V are shown in Figure 9.

It can be seen from the figure that under the same laser voltage, the plasma temperature generated on the surface of the sample is also different. The main reason is that there is an error in the laser itself, and even at the same laser pulse voltage, the emitted laser pulse energy is not exactly the same due to the presence of oscillations. When the laser is fixedly focused on the burning spot on the sample surface, the plasma state produced by the laser pulse burning the sample changes. In order to obtain a calibration curve with a fixed plasma temperature, it is necessary to continuously move the sample so that the laser burns on a different surface of the sample each time.

In the experiment, the characteristic peaks of Ti I454 nm and Si I288.76 nm were selected as the calibration curve of Ti. The experimental samples are 6 groups of samples from *S*1 to *S*6, the laser amplification voltage is 300 V, the laser pulse frequency is set to 10 Hz, the spectrometer integration time is 25 ms, and the average is 25 times. The obtained calibration curve is shown in Figure 10(a) (left). The fitting straight line formula obtained is $Y = 0.0084X + 0.016$, its linear coefficient $R2 = 0.92$, and the relative error is 8.9%.

In order to keep the plasma temperature basically constant, it is necessary to move the laser to burn the sample point and observe the intensity ratio of the two spectral lines of Si I28.76 nm and Si I251.4 nm to indirectly observe the plasma temperature. In the experiment, the laser voltage was adjusted slightly to make the plasma temperature of different samples roughly the same, and the data points under the selected laser voltage were fitted. The experimental samples are 6 groups of samples from *S*1 to *S*6. The laser amplification voltage is about 300 V, the laser pulse frequency is set to 10 Hz, the spectrometer integration time is 25 ms, and the average is 25 times. The calibration curve obtained by fitting is shown in Figure 10(b). The calibration curve formula $Y = 0.0129X + 0.01347$, its linear correlation coefficient $R2 = 0.985$, and the relative error is 5.3%.

By comparing the two curves, it can be found that the Ti calibration curve obtained with a fixed plasma temperature has better linearity than the Ti calibration curve obtained with a constant laser voltage. This is because the fixed plasma temperature method satisfies the assumption of local thermodynamic equilibrium required for quantitative analysis. It also reduces the influence of matrix effects on LIBS quantitative analysis. At the same time, it was found that the calibration curves of the two did not pass the origin, indicating that the fixed plasma method also has a certain detection limit for the content test of trace elements.

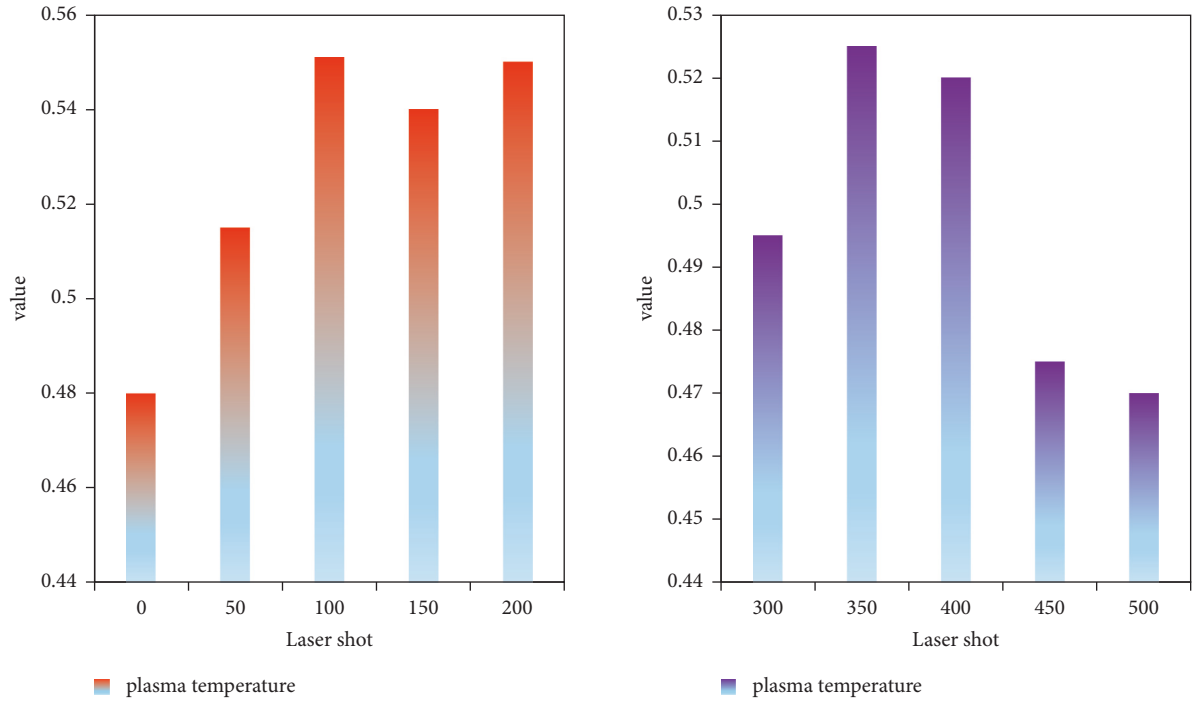

Figure 9: Plasma temperature variation at 300 V.

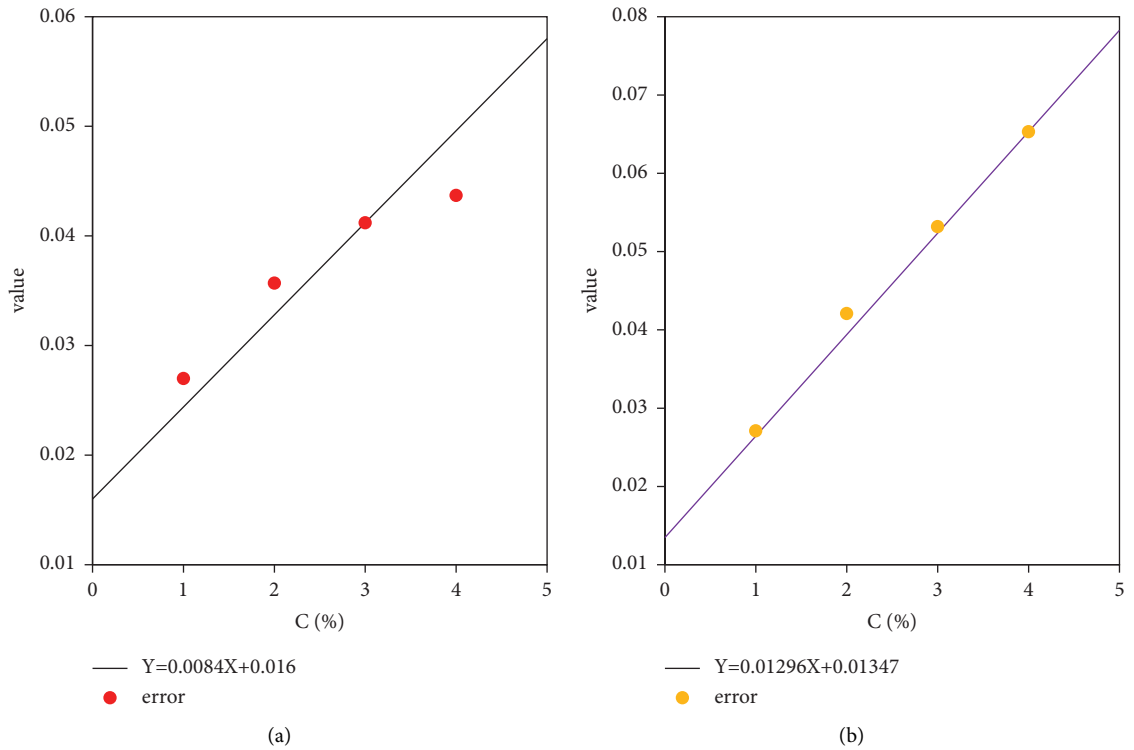

Figure 10: (a) The calibration curve obtained by fixing the laser pulse voltage (left). (b) Ti calibration curve obtained by the fixed plasma temperature method (right).

5. Conclusion

Multitarget tracking technology is an important subject in computer vision technology. According to the detected object, it matches the existing orbit data and combines it with features such as appearance, state, and position to achieve multitarget tracking. The purpose of this paper is to quantitatively analyze atomic spectra based on laser-induced teaching fused with multitarget tracking algorithms. The Al_2O_3-TiO_2 sample was qualitatively analyzed by LIBS, and

the titanium and aluminum elements other than oxygen in the sample could be detected by analyzing the emission spectrum obtained. The effects of cautery conditions and laser pulse energy on plasma temperature were investigated. The results show that the plasma temperature change of the emission spectrum obtained by keeping the laser burning position unchanged is larger than the plasma temperature change of the emission spectrum obtained by moving the laser burning point in real time. The plasma temperature showed an increasing trend with the increase of laser pulse energy. As an important technology for composition analysis, laser-induced breakdown spectroscopy has the advantages of high sensitivity and fast real time and other advantages in the detection of material composition content. Due to the limitations of time and technology, we have not conducted in-depth research on the fusion of multitarget tracking algorithms in laser-induced breakdown spectroscopy technology, and we will conduct more in-depth research and analysis in the future.

Data Availability

The data used to support the findings of this study can be obained from the corresponding author upon request.

Conflicts of Interest

The authors declare that they have no conflicts of interest.

Acknowledgments

This research study was sponsored by (1) Jilin Provincial Association of Higher Education: Research on teaching mode of College Physical Optics Experiment Course based on Internet+, project no. JGJX2021D101, and (2) Changchun University of Science and Technology, Research on teaching mode of College Physical Experiment based on network, project no. XJY2004.

References

[1] Y. Liu, M. R. Ward, and A. J. Alexander, "Polarization independence of laser-induced nucleation in supersaturated aqueous urea solutions," *Physical Chemistry Chemical Physics*, vol. 19, no. 5, pp. 3464–3467, 2017.

[2] S. Khan, S. Bashir, and A. Hayat, "laser-induced breakdown spectroscopy of tantalum plasma additional information on phys. plasmas laser-induced breakdown spectroscopy of tantalum plasma," *Environmental Monitoring and Assessment*, vol. 136, no. 1-3, pp. 391–399, 2017.

[3] S. Lepeshov, A. Krasnok, I. Mukhin et al., "Fine-tuning of the magnetic Fano resonance in hybrid oligomers via fs-laser-induced reshaping," *ACS Photonics*, vol. 4, no. 3, pp. 536–543, 2017.

[4] Y. J. Yan, L. L. Bao, L. J. Zhang et al., "Inhibition of laser-induced choroidal neovascularization by hematoporphyrin dimethylether-mediated photodynamic therapy in rats," *Biological & Pharmaceutical Bulletin*, vol. 40, no. 12, pp. 2088–2095, 2017.

[5] Y. Wang, M. R. Zhou, P. C. Yan, and C.D. He, "Identification of coalmine water inrush source with PCA-BP model based on laser-induced fluorescence technology," *Guang pu xue yu guang pu fen xi = Guang pu*, vol. 37, no. 3, pp. 978–983, 2017.

[6] H. Zhang, Y. Sun, S. Li, W. Shi, and C. Feng, "Long-term tracking based on multi-feature adaptive fusion for video target," *IEICE - Transactions on Info and Systems*, vol. E101.D, no. 5, pp. 1342–1349, 2018.

[7] J. Zhang, D. Zhang, and J. Wan, "A new video tracking algorithm based on multi-complementary features fusion," *Xibei Gongye Daxue Xuebao/Journal of Northwestern Polytechnical University*, vol. 37, no. 2, pp. 323–329, 2019.

[8] Y. Li, Z. He, S. Wang, Z. Wang, and W. Huang, "Multideep feature fusion algorithm for clothing style recognition," *Wireless Communications and Mobile Computing*, vol. 2021, no. 4, pp. 1–14, 2021.

[9] L. He, G. Liu, G. Tian, J. Zhang, and Z. Ji, "Efficient multi-view multi-target tracking using a distributed camera network," *IEEE Sensors Journal*, vol. 20, no. 4, pp. 2056–2063, 2020.

[10] X. Ma, "Fixed-point tracking of English reading text based on mean shift and multi-feature fusion," *Journal of Intelligent and Fuzzy Systems*, vol. 40, no. 4, pp. 6315–6325, 2021.

[11] L. A. Shelukhin, V. V. Pavlov, P. A. Usachev, P. Y. Shamray, R. V. Pisarev, and A. M. Kalashnikova, "Ultrafast laser-induced changes of the magnetic anisotropy in a low-symmetry iron garnet film," *Physical Review B: Condensed Matter*, vol. 97, no. 1, p. 014422, 2018.

[12] E. H. Lee and T. L. Song, "Multi-sensor track-to-track fusion with target existence in cluttered environments," *IET Radar, Sonar & Navigation*, vol. 11, no. 7, pp. 1108–1115, 2017.

[13] L. Liu, H. Ji, W. Zhang, and G. Liao, "Multi-Sensor multi-target tracking using probability hypothesis density filter," *IEEE Access*, vol. 7, no. 99, pp. 67745–67760, 2019.

[14] M. W. . Sasieni, "Marketing and management science: a synergism," *Journal of the Operational Research Society*, vol. 22, no. 2, pp. 190-191, 2017.

[15] Z. Li, X. Li, M. Shi et al., "Tracking algorithm of snowboard target in intelligent system," *Journal of Intelligent and Fuzzy Systems*, vol. 40, no. 2, pp. 3117–3125, 2021.